Turbulent Flow Control using Wall Sensing

Anushka Subedi* and Yulia Peet†

School for Engineering of Matter, Transport and Energy, Arizona State University, Tempe, AZ, 85281

Turbulent flow control plays a pivotal role in diverse applications such as drag reduction, mixing, heat transfer, and boundary layer and flow separation control. Although numerous active and passive methods have been explored for mitigating drag in turbulent flows, this study introduces an approach, not widely explored, that utilizes wall-sensing based on wall shear stress. We conduct a comparative analysis with the opposition control method, which uses velocity sensing at an off-wall location. The results from opposition control reveal significant drag reduction: 21.11% at $Re_{\tau}\approx$ 180 and 18% at $Re_{\tau}\approx$ 390. In contrast, the wall-sensing method achieves drag reductions of 10.64% at $Re_{\tau}\approx$ 180 and 7.12% at $Re_{\tau}\approx$ 390. This relative ineffectiveness of the wall-sensing control method is attributed to a high-frequency content of the wall shear stress data, which, if undamped, may lead to oscillations in the applied control signal. This, in turn, requires either a reduction in gain, or 'freezing' of the control input in time to arrive at a stable control implementation, reducing the method effectiveness as compared to an opposition control approach.

I. Nomenclature

 Re_{τ} = friction Reynolds number

 U_{bulk} = bulk mean velocity

CFL = Courant–Friedrichs–Lewy condition

 Δt = time-step size

DNS = Direct Numerical Simulation

d = vertical location of sensing plane in opposition control

 u_x = streamline velocity u_y = vertical velocity

v = kinematic viscosity of the fluid $\tau_w = v \frac{\partial u_x}{\partial v}$ = instantaneous wall shear stress

DR = drag reduction

 U_{mean} = average value of streamwise velocity u'u' = Reynolds velocity stress term in x-direction $v'v' = u'_y u'_y$ = Reynolds velocity stress term in y-direction w'w' = Reynolds velocity stress term in z-direction

u'v' = Reynolds shear stress term P_{mean} = average value of pressure p'p' = pressure fluctuations term

u'p' = correlations between velocity fluctuations in x-direction and pressure v'p' = correlations between velocity fluctuations in y-direction and pressure

A = control gain

II. Introduction

The presence of drag is undesirable in many engineering applications, including aerospace, automotive, and marine systems, due to its association with increased energy consumption and reduced efficiency. To address this issue, various active control strategies have been explored, such as blowing and suction [1-3], synthetic jets [4, 5], and fluidic

^{*}Ph.D. Student, AIAA member, email: asubedi5@asu.edu

[†]Associate Professor, AIAA member, email: ypeet@asu.edu

oscillators [6], all of which require energy input and involve complex control systems. Conversely, passive control strategies, including retrofits and compliant surfaces [7], and recently, metamaterials [8], have been investigated for drag mitigation without additional energy expenditure. For such passive control technologies, optimizing the response of passive surfaces like metamaterials to fluid loading requires feedback based on wall quantities such as pressure and wall shear stress. In this study, we explore the wall-sensing control method by utilizing the wall shear stress and conduct a comparative analysis with the opposition control method, which utilizes velocity sensing across an off-wall location.

There have been a significant number of investigations into opposition control techniques for turbulent flow control [1, 9–12]. Choi, Moin, and Kim [1] were the first to introduce the idea of the opposition control and to investigate this strategy in a turbulent channel flow using direct numerical simulation. In the opposition control by [1], the transpiration velocity at the wall is supplied as being equal in magnitude and opposite in sign to a vertical velocity measured at an off-wall plane parallel to the wall and separated from it by a certain distance. They achieved skin-friction drag reduction of approximately 25% with the opposition control method for bulk Reynolds number of approximately 1800 (based on channel half-width). An opposition control study that only uses blowing and not suction was done by [10], where they were able to achieve a substantial drag reduction of 60.8% in a turbulent boundary layer at $Re_{\tau} \approx 960$. However, this strategy does not conserve the mass flux and introduces a non-zero net mass flow rate, which might pose a limitation for practical applications. In a study by [9], an active wall motion control of channel flow at $Re_{\tau} \approx 140$ is performed based on the opposition control laws to mitigate skin friction drag. They locally deformed the wall based on two feedback control strategies; one that induces wall motion opposing the wall-normal velocity (opposition control) and another proportional to the spanwise derivative of the spanwise velocity gradient at the wall. These methods yielded drag reductions ranging from 13% to 17% (with opposition control giving higher drag reduction values than a control based on the spanwise derivative of the spanwise velocity gradient). While the opposition control strategies that utilize the vertical velocity at an off-wall sensing location have significant drag reductions, they are impractical because such information isn't typically available. This makes the need of using something more practical for implementing the control like wall-measurable quantities.

As an alternative to impractical wall-normal velocity control, a wall-based control is also studied by the same work of Choi, Moin and Kim [1], where they used joint probability density functions to analyze correlations between wall variables and flow structures above the wall, including wall pressure and derivatives of streamwise and spanwise velocity gradients at the wall. Despite efforts, correlations between these variables and flow events above the wall were limited and the best they could achieve was 6% reduction in skin-friction drag. Lee, Kim, and Choi [11] conducted a study applying suboptimal control theory to turbulent channel flow for drag reduction. They developed simple feedback control laws based on spanwise derivatives of pressure or spanwise velocity gradient at the wall, evaluated in Fourier space, and demonstrated that these laws could achieve a 16-22% reduction in skin-friction drag at Re_{τ} = 110. They achieved a significant drag reduction but their method is still impractical to implement because it is done in Fourier space. Moreover, it is based on evaluating spanwise derivatives of wall quantities, which are not easily obtained from wall sensors nor they can be sensed by passive surfaces or metamaterials. The same can be said about the study of [9] who also implemented control based on a spanwsie derivative of the wall velocity gradient. In our study, we also study flow control using the wall information (wall shear stress) by replicating a constant-gain opposition-type response as in the wall-normal velocity control. Our control strategy is implemented in physical space and is based on the shear stresses themselves, and not their derivatives, thus making it practicable for implementation with metamaterials that would sense the fluid forces (such as shear stress), and not their derivatives. This approach ensures effective modulation of turbulent flow dynamics in the context of a surface response to fluid loading (through transpiration).

In this study, we implement the control in a turbulent channel with the domain of $2\pi h \times 2h \times \pi h$, with h being the channel half-width. The boundary conditions are periodic in streamwise and spanwise directions and use no-slip at the walls, for the uncontrolled case. In the controlled cases, vertical wall transpiration velocity is applied to the bottom wall, while no-slip is used at the top wall. The choice of the channel flow configuration for this work is deliberate, influenced by the abundance of available research for comparison and its suitability as a foundational framework for our novel method. This selection not only facilitates ease of implementation but also lays a robust groundwork for extending our investigation into passive control utilizing metamaterials across diverse geometries. We explore the flow regimes at the friction Reynolds numbers of $Re_{\tau} \approx 180$ and $Re_{\tau} \approx 390$. This research presents insights into drag reduction techniques, providing potential advancements for more energy-efficient and effective strategies in engineering applications.

III. Numerical Method

Flow control simulations are executed using the Spectral Element code, Nek5000 [13–15], which is a high-order solver that utilizes polynomial basis functions associated with Gauss-Lobatto-Legendre points defined on the elements, ensuring efficient tensor-product utilization and rapid convergence. In this research, the computational grid (for all cases) uses $16 \times 12 \times 8$ number of elements, each containing 8^3 Gauss-Lobatto-Legendre collocation points, with a polynomial order of N=7 in the simulations. The bulk mean velocity, U_{bulk} , remains constant throughout the simulations, achieved by an application of a body force adaptively adjusted via a proportional feedback control loop [13]. The time-step size is set to maintain a constant CFL number of 0.5 and fluctuates slightly around the value of $\Delta t = 10^{-4}$. The uncontrolled case is initialized from a turbulent channel mean velocity profile superimposed by velocity fluctuations defined at certain wave-numbers, and the controlled cases are initialized from a fully-developed uncontrolled case at the corresponding Re_{τ} . To validate the uncontrolled base case, comparisons are made against the DNS data from [16].

A. Opposition Control

For the opposition control, we use the instantaneous wall velocity signal $u_y(x, y = d, z, t)$, taken from a specified wall-normal plane, located at the distance d from the lower wall, and resupply it with the opposite sign as the velocity at the lower wall, directly underneath the sensed location:

$$u_y|_{wall}(x, z, t) = u_y(x, y = 0, z, t) = -u_y(x, y = d, z, t).$$
 (1)

Following the previous literature on the opposition control method [1, 11, 17–19], we investigate the values of the sensing plane location as $y^+ = 5$, 10, 15 and 20. The idea of the opposition control is based on the hypothesis that a negative (positive) vertical velocity fluctuation near the wall signifies of a passing of a turbulent sweep (ejection) event, which can be effectively interfered with (opposed) by a local positive (negative) wall transpiration [1].

B. Wall-Sensing Method

For the wall-sensing method, we have utilized the following flow control relation:

$$u_{y|_{wall}}(x,z,t) = A \times \left[\left(v \frac{\partial u_{x}}{\partial y} \right)_{wall}(x,z,t) - \left(v \frac{\partial u_{x}}{\partial y} \right)_{wall}(t) \right] \times \frac{\sqrt{\langle u'_{y}u'_{y} \rangle}_{y=d}^{no-control}}{\sqrt{v^{2} \left(\frac{\partial u'_{x}}{\partial y} \frac{\partial u'_{x}}{\partial y} \right)_{wall}^{no-control}}}$$
(2)

Here, $u_y|_{wall}(x,z,t)$ is the instantaneous vertical velocity at the wall, $\left(v\frac{\partial u_x}{\partial y}\right)_{wall}(x,z,t)$ is the instantaneous shear stress at the wall, $\sqrt{\langle u'_y u'_y \rangle}_{y=d}^{no-control}$ is the square root of the Reynolds stress term in the y-direction at a specified wall-normal location y=d taken from the uncontrolled case with the same Reynolds number, $\sqrt{v^2\left(\frac{\partial u'_x}{\partial y}\frac{\partial u'_x}{\partial y}\right)_{wall}^{no-control}}$ is the averaged wall shear stress fluctuation taken from the uncontrolled case (angular brackets denote time and plane averaging), and A is the amplitude (gain) of the control. This last term in Eq. (2), $\frac{\sqrt{\langle u'_y u'_y \rangle}_{y=d}^{no-control}}{\sqrt{v^2\left(\frac{\partial u'_x}{\partial y}\frac{\partial u'_x}{\partial y}\right)_{wall}^{no-control}}$, scales the control input for the wall velocity in accordance with the opposition control law. The velocities in the x and z direction at the wall are set to zero. We note

accordance with the opposition control law. The velocities in the x and z direction at the wall are set to zero. We note that Eq. (2) satisfies a zero-net flux condition across the wall at every time instance.

The idea behind the proposed control law in Eq. (2) stems from the fact that positive shear stress fluctuations are associated with the passing of local turbulent sweep events and need to be counteracted with the positive transpiration velocity (blowing) [1]. Conversely, local negative shear stress events are associated with turbulent ejections that need to be counteracted by suction. These ideas are reminiscent of the opposition control strategy and explain why the positive sign in front of the control gain A in the feedback loop is used in the wall-sensing control based on local shear stresses in Eq. (2). Positive values of A should result in drag reduction, while negative values of A in drag increase, which is confirmed in the present study as discussed in the next section.

IV. Results

The reduction in drag is measured to test the effectiveness of the control methods. Here, drag is defined as the plane-averaged value of wall shear stress,

$$\tau_w(t) = \overline{\left(v\frac{\partial u_x}{\partial y}\right)_{wall}}(t). \tag{3}$$

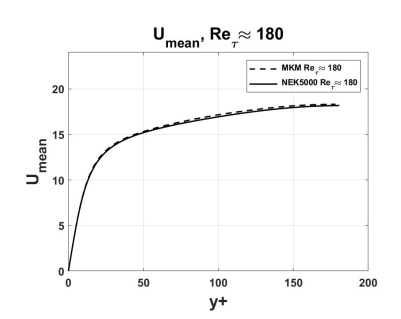
The skin friction drag reduction is defined as

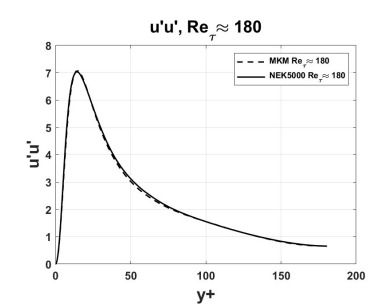
$$DR = \frac{\int_{T_1}^{T_2} \left(\tau_w^{no-control}(t) - \tau_w(t)\right) dt}{\int_{T_1}^{T_2} \tau_w^{nc}(t) dt} \cdot 100\%,\tag{4}$$

where $\tau_w^{no-control}(t)$ represents the uncontrolled case, while $\tau_w(t)$ denotes the controlled case. For the opposition control, the values $T_1 = 50$ and $T_2 = 400$, normalized by h/U_{bulk} , indicate the beginning and the end of the period during which statistics are collected (the value of $T_1 = 50$ is used to allow for a flow adjustment from synthetic turbulent initial conditions). For the wall-sensing control, the beginning and the end of the statistics collection time are $T_1 = 0$ and $T_2 = 400$, since the fully-developed turbulence is used as initial conditions for the controlled cases.

A. Turbulent Channel Flow Benchmark

The uncontrolled turbulent channel base code has been validated against DNS data, as collected by Moser, Kim and Mansour in [16] (referred to as 'MKM' data). In Fig. 1 to Fig. 5, turbulent statistics, including U_{mean} , u'u', u'v', v'v', and w'w' for $Re_{\tau} \approx 180$ are presented and compared to the MKM data. Additional turbulent statistics with pressure terms for $Re_{\tau} \approx 180$ relative to the MKM data are provided in the appendix.





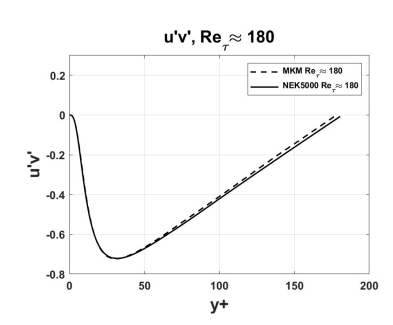


Fig. 1 U_{mean} against MKM data [16]

Fig. 2 u'u' against MKM data [16]

Fig. 3 u'v' against MKM data [16]

150

200

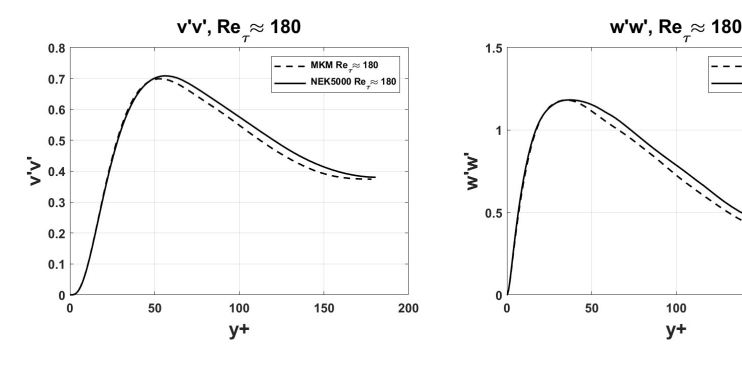
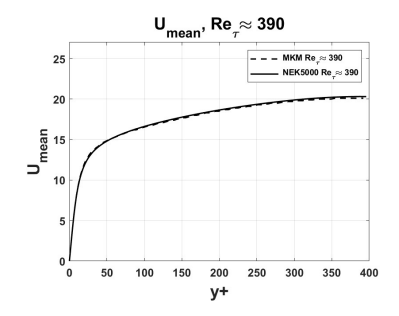
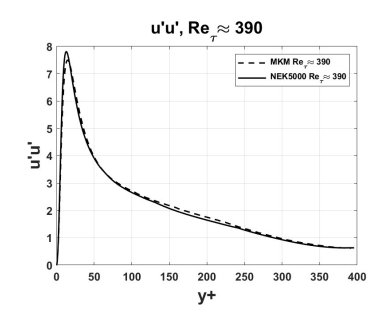


Fig. 4 v'v' against MKM data [16] Fig. 5 w'w' against MKM data [16]

The turbulent statistics for $Re_{\tau} \approx 180$ show a good level of consistency with the MKM data. Similarly, Fig. 6 to Fig. 10 showcase turbulent statistics, i.e., U_{mean} , u'u', u'v', v'v', and w'w' for $Re_{\tau} \approx 390$, comparing them to the MKM data in [16]. Supplementary turbulent statistics pertaining to $Re_{\tau} \approx 390$ in relation to the MKM data are provided in the

appendix, similar to the $Re_{\tau} \approx 180$ case. The collected statistics are time converged for Reynolds number regimes. for The turbulent statistics exhibit a notable consistency with the MKM data with some marginal errors for both friction Reynolds numbers, showing the reliability of the results.





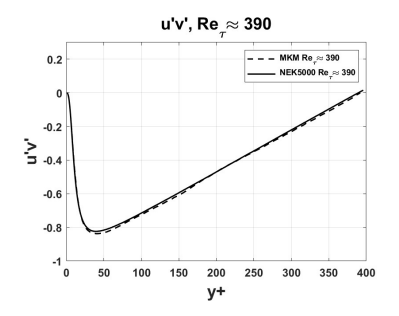
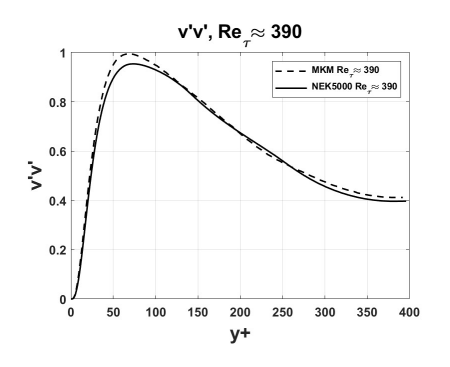


Fig. 6 U_{mean} against MKM data [16]

Fig. 7 u'u' against MKM data [16]

Fig. 8 u'v' against MKM data [16]



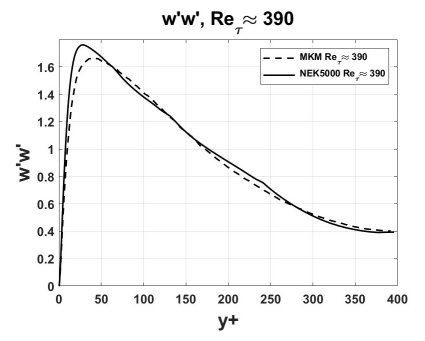
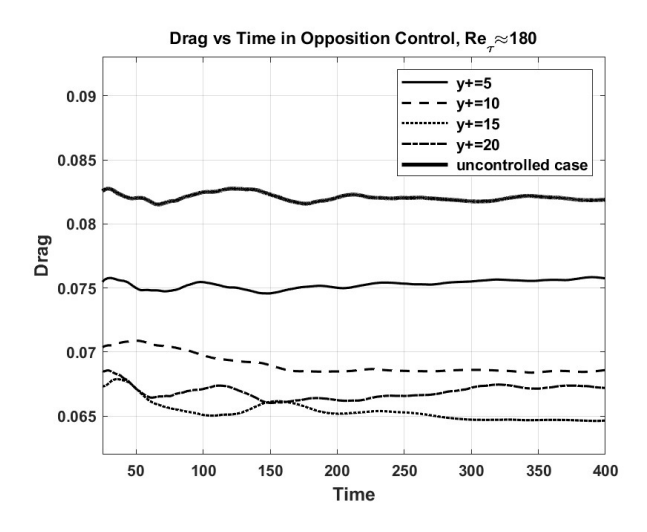


Fig. 9 v'v' against MKM data [16] Fig. 10 w'w' against MKM data [16]

B. Opposition Control

In Fig. 11, we observe the temporal evolution of drag, comparing the uncontrolled state at $Re_{\tau} \approx 180$ with controlled cases. We choose the location of the sensing plane as $y^+ = 5$, 10, 15, and 20, and compare between different cases. The results show maximum drag reduction when capturing instantaneous velocity at y^+ value of 15, followed by decreasing order for y^+ values of 20, 10, and 5, which is consistent with the previous literature [17–19].

In Fig. 12, we illustrate the percentage drag reduction for $Re_{\tau} \approx 180$ with the sensing location of $y^+ = 5$, 10, 15, and 20. The findings show the most effective percentage of drag reduction occurring at a y^+ value of 15, with a notable reduction of 21.11%. This is followed by a descending order of effectiveness for y^+ value of 20 with 17.94% DR, y^+ value of 10 with 16.35% DR, and y^+ value of 5 with 7.56% DR.



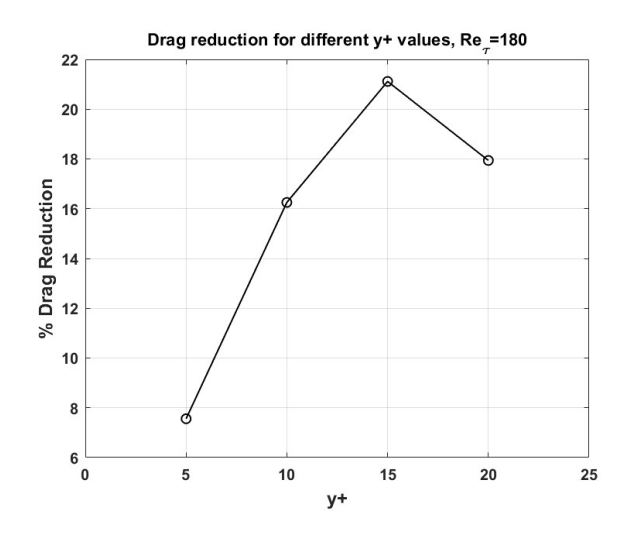
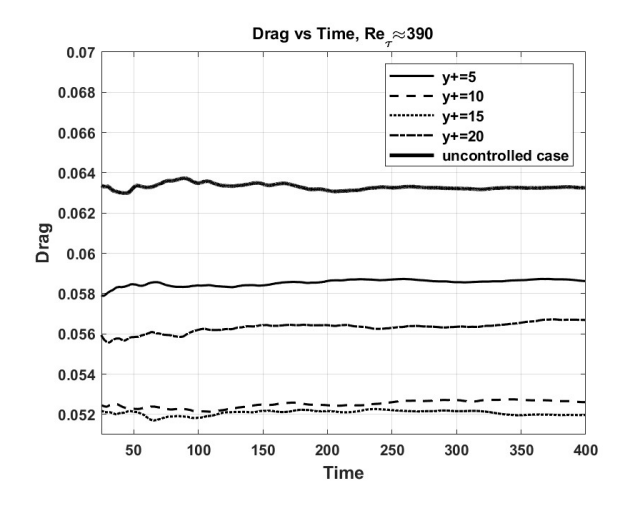


Fig. 11 Temporal evolution of drag for $Re_{\tau} \approx 180$

Fig. 12 Drag reduction vs y^+ values for $Re_{\tau} \approx 180$

In Fig. 13, we present the temporal evolution of drag for $Re_{\tau} \approx 390$. Similar to the observations in the $Re_{\tau} \approx 180$ case, the maximum reduction in drag is noted at a sensing plane location of $y^+ = 15$. However, a notable difference from the previous case is observed, as the second-best location for drag reduction is identified at $y^+ = 10$ instead of $y^+ = 20$.

In Fig. 14, we present the percentage drag reduction for $Re_{\tau} \approx 390$, analyzing sensing plane locations at y^+ values of 5, 10, 15, and 20. The results highlight the most significant percentage drag reduction at y^+ value of 15, exhibiting an 18% reduction. This is followed by a descending order for y^+ value of 10 with 16.90% DR, y^+ value of 20 with 10.58% DR, and y^+ value of 5 with 7.42% DR.



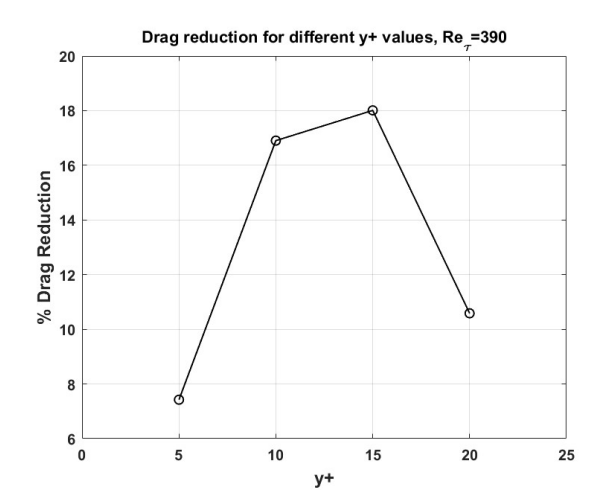


Fig. 13 Temporal evolution of drag for $Re_{\tau} \approx 390$

Fig. 14 Drag reduction vs y^+ values for $Re_{\tau} \approx 390$

Comparing our findings with previous research on opposition control, we note similar values of maximum drag reduction of 25% reported in [1] for $Re_{\tau} = 180$, and 16–22% reported in [11] for $Re_{\tau} = 110$. Additionally, a sensitivity of drag reduction to the sensing plane location, as well as an optimal value of $y^+ = 15$ for a similar range of Reynolds numbers was previously reported in [17–19]. Our results align well with these observations.

C. Wall-Sensing Control

In Fig. 15, we observe the evolution of drag over time for $Re_{\tau} \approx 180$ for the wall-sensing method, compared with the uncontrolled case. Initially, we applied a control gain A=1 in Eq. (2), which resulted in a very low drag reduction value of only 2.93% at $Re_{\tau} \approx 180$. For greater drag reduction, we incrementally increased the control gain.

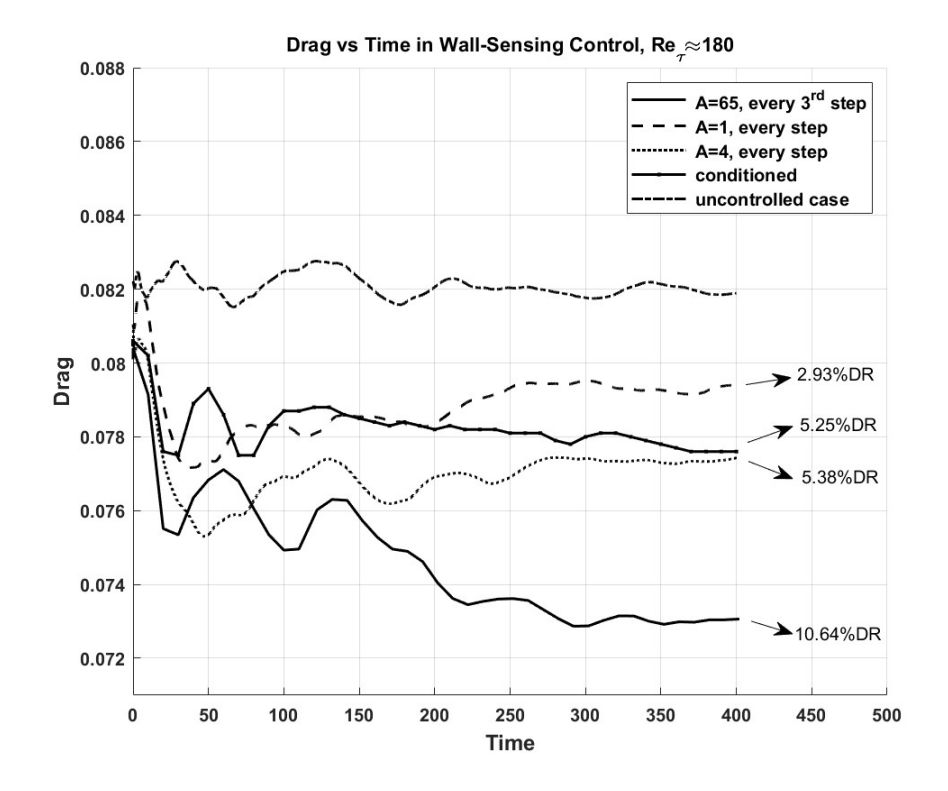


Fig. 15 Temporal evolution of drag, $Re_{\tau} \approx 180$

Upon raising the control gain to A=4, we observed a noticeable improvement, achieving a higher drag reduction value of 5.38% at $Re_{\tau}\approx 180$. However, increasing the gain further led to an instability in the system. Specifically, beyond A=4, the control mechanism could no longer maintain a stable operation, causing fluctuations and overshoots in the supplied wall velocity that negated the benefits of drag reduction. To address this challenge and stabilize the control system, we implemented a 'freeze' technique. This approach involved holding the control input fixed for three time steps and then reapplying the control input, repeating this cycle over time. By employing the 'freeze' technique, we managed to significantly enhance the stability of the system. This method allowed us to increase the gain to a much higher value, specifically up to A=65. The implementation of this higher gain, with a periodic freezing for every three time steps, resulted in a substantial improvement in drag reduction with 10.64% drag reduction at $Re_{\tau}\approx 180$.

Similar to the $Re_{\tau} \approx 180$ case, in Fig. 16, we observe the evolution of drag over time for $Re_{\tau} \approx 390$ using the wall-sensing method. The results for $Re_{\tau} \approx 390$ also show varying levels of drag reduction depending on the control gain applied. At a control gain of A=1, we achieved a drag reduction of 1.12%. Increasing the control gain to A=4 resulted in a more substantial drag reduction of 3.48%. However, similar to the observations at $Re_{\tau} \approx 180$, further increasing the control gain led to instability in the system. To address this, we employed the 'freeze' technique and the method allowed us to manage higher gains more effectively, achieving a drag reduction of 7.12% at $Re_{\tau} \approx 390$.

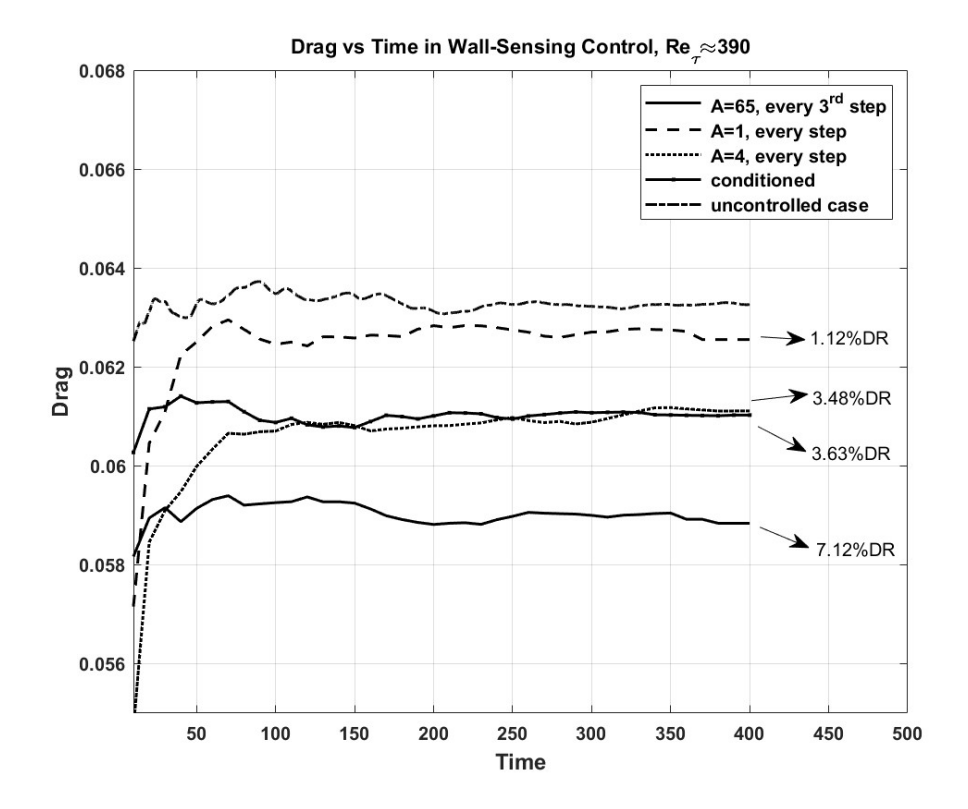


Fig. 16 Temporal evolution of drag, $Re_{\tau} \approx 390$

In addition to varying the control gains and implementing a 'freeze' technique, another control approach was also investigated. This involved first computing the control signal as would be given by Eq. (2),

$$u_{y,control}(x,z,t) = A \times \left[\left(v \frac{\partial u_x}{\partial y} \right)_{wall} (x,z,t) - \overline{\left(v \frac{\partial u_x}{\partial y} \right)_{wall}} (t) \right] \times \frac{\sqrt{\langle u_y' u_y' \rangle}_{y=d}^{no-control}}{\sqrt{v^2 \left(\frac{\partial u_x'}{\partial y} \frac{\partial u_x'}{\partial y} \right)_{wall}^{no-control}}},$$
 (5)

and then conditioning this control signal by the sign of the vertical velocity at y = d as

$$u_{y}|_{wall}(x,z,t) = \begin{cases} u_{y,control}(x,z,t), & \text{if } u_{y,control}(x,z,t) \times u_{y}(x,y=d,z,t) < 0\\ 0, & \text{otherwise} \end{cases}$$
 (6)

This approach is referred to as 'conditioned' in the plots. The purpose of this condition is to ensure that the control law faithfully follows the opposition control condition, i.e. the injected wall velocity is of the opposite sign to the sensed vertical velocity at the off-wall location. The 'conditioned' approach utilized the gain value of A=5 for both $Re_{\tau}\approx 180$ and 390 (the highest we could implement without facing the instabilities), the location of the sensing plane d corresponding to $y^+=15$ in Eq. (6), and no freezing was used. Despite the fact that the 'conditioned' approach satisfied the opposition control velocities sign convection, it did not result in significant improvements in the wall-sensing method. This control yielded a drag reduction of 5.25% at $Re_{\tau}\approx 180$ and 3.63% at $Re_{\tau}\approx 390$. The study also explored the effects of applying negative gains (i.e. A having negative values) in the wall-sensing control, it resulted in drag increase in the wall-sensing control, as expected.

To summarize, in Fig. 17 and Fig. 18 we compare the best performing wall-sensing method (which is A = 65 with 'freezing') with the best-performing opposition control method (with $y^+ = 15$) for $Re_{\tau} = 180$ and 390, respectively. While the advantages of the opposition control approach are clear, the wall-sensing methods, based exclusively on the local wall information that can be sensed actively by wall sensors or passively by 'smart' control surfaces (such as selectively-tuned compliant surfaces or metamaterials) still demonstrate a significant drag reduction.

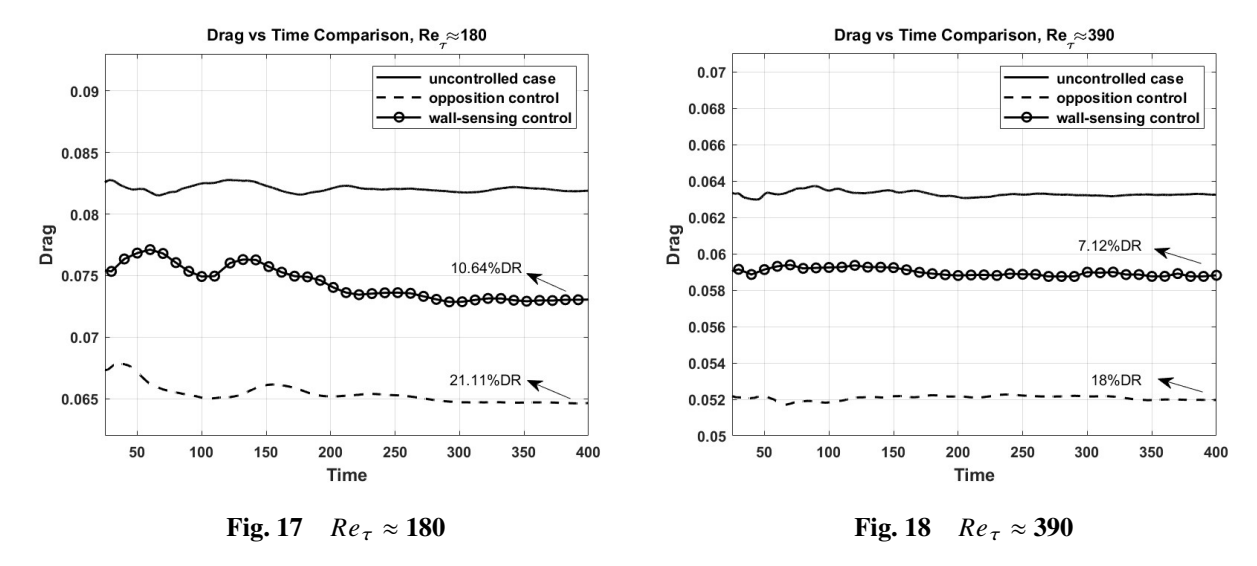


Fig. 17 and 18: Comparison between uncontrolled case, and best performing opposition control and wall-sensing control methods

To understand why the wall-sensing method appears to be less effective than the opposition control method, we analyzed the variation of the control input (i.e. the injected wall velocity) with time as control is applied for both methods. Fig. 19 and Fig. 20 present the control value at the wall for both control strategies at a selected (x, z) location. These figures compare the supplied control value with the vertical velocity signal at $y^+ = 15$ of the uncontrolled case, taken with a minus sign, at the same (x, z) location. Based on the ideas from the opposition control strategy, in theory, the supplied control signal should track the negative of the off-wall vertical velocity with a high level of correlation. In Figs. 19 and 20, both control methods apply control inputs at every time step. In the case of the wall-sensing method investigated in Fig. 20, a control gain of A = 5 was used, which is just above the instability threshold. The reason for this choice of gain was to investigate a potential cause of instability.

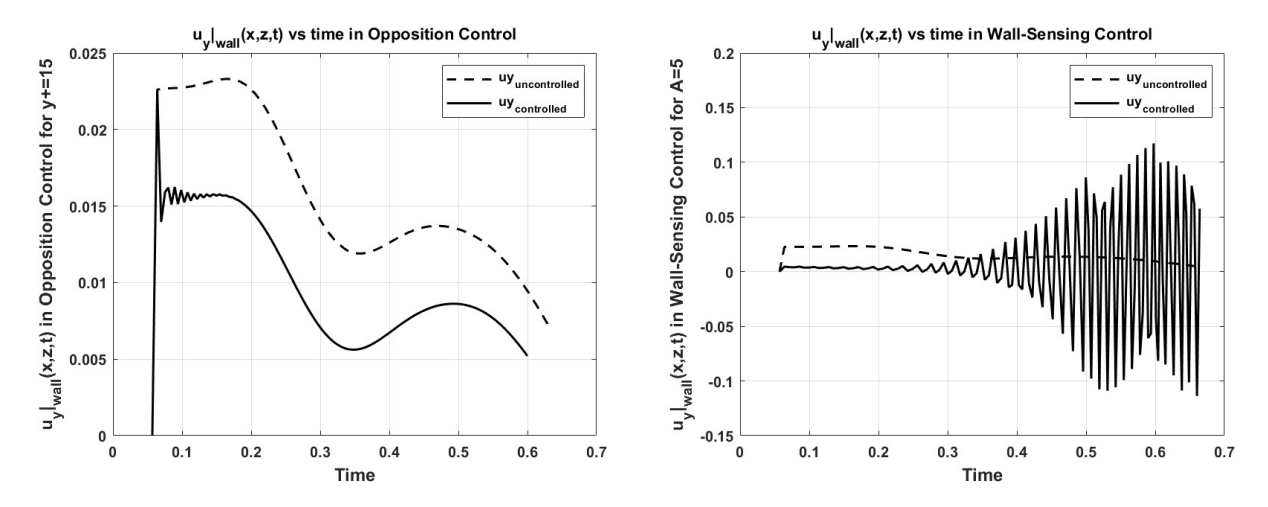


Fig. 19 Control velocity in opposition control

Fig. 20 Control velocity in wall-sensing control

Fig. 19 and 20: Comparison between the input wall velocity (solid line) and the negative of the wall-normal velocity in the uncontrolled case (dashed line) taken at $y^+ = 15$, with opposition (for $y^+ = 15$) and wall-sensing (for A = 5) control methods. Control is applied at the time t=0.06.

In opposition control, the control value quickly stabilizes after some initial small fluctuations and maintains a steady, smooth trajectory throughout the control process. The applied control signal tracks the (negative of) vertical velocity at

 y^+ = 15 very well, albeit manifests slower values. This is because the vertical velocity for comparison is taken from the uncontrolled case: with the application of control, its fluctuating value reduces due to drag reduction. However, when employing the wall-sensing control method, we observe oscillations in the control value, resulting in instability. This oscillatory behavior of the wall-sensing control method can be traced back to the high-frequency outliers present in the wall shear stress data (in a sense that the oscillations first appear locally, at the spatial locations where strong shear stress fluctuations are observed). These local outbursts of instability in the controlled case eventually spread out, affecting the whole system.

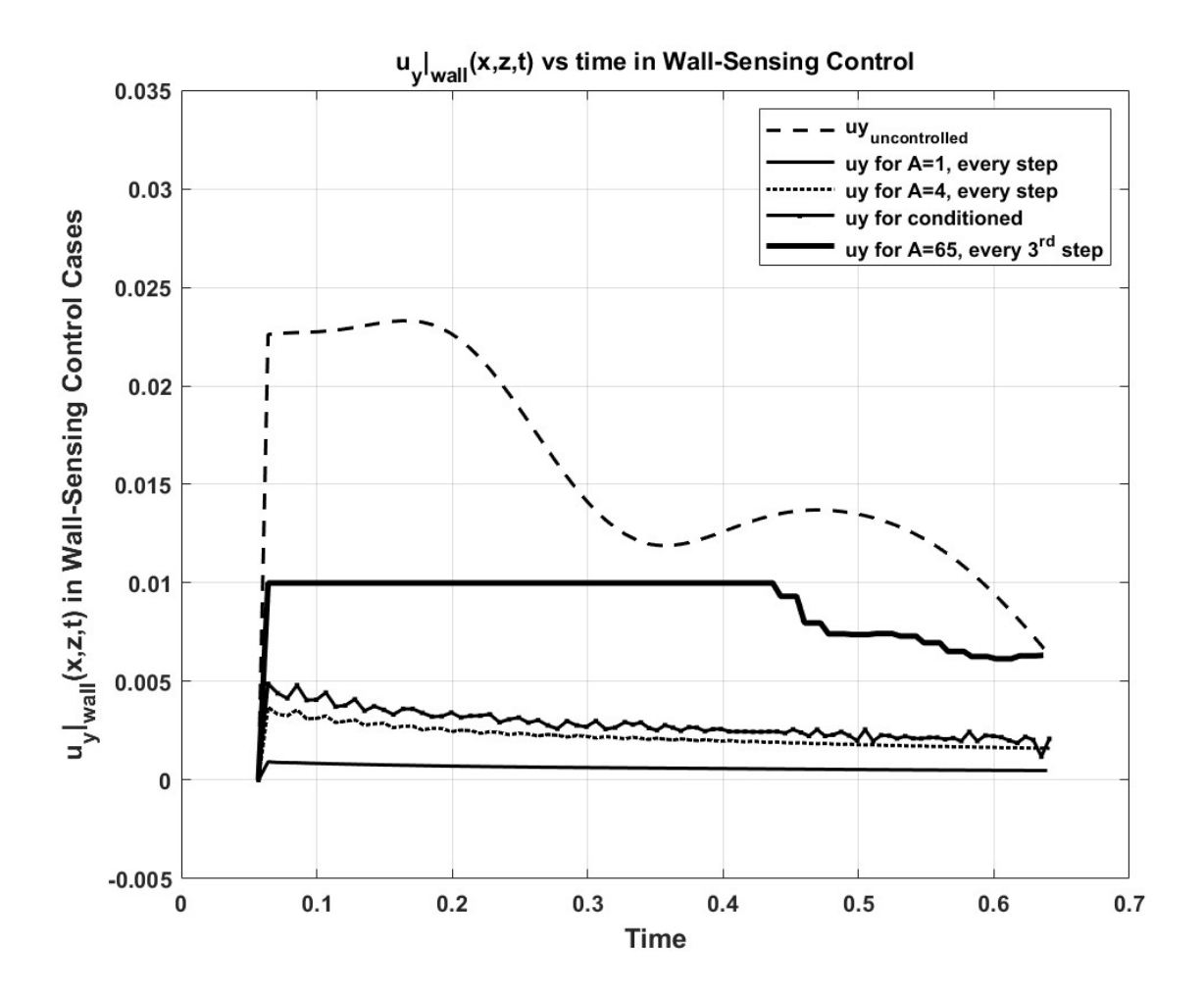


Fig. 21 Control velocity in stable wall-sensing cases as compared to the negative of the vertical velocity at $y^+ = 15$ from the uncontrolled case.

Fig. 21 illustrates how control velocities vary in stable wall-sensing cases with different gain values: A = 1, A = 4, the 'conditioned' case, and the A = 65 'freeze' case. This comparison gives us insight of why the wall-sensing control with low gain values results in a less effective method than the opposition control with the unit gain. Fig. 21 shows that, despite the normalization in Eq. (2), introduced in an attempt to match the supplied control input in wall-sensing method with the off-wall vertical velocity in magnitude (to mimic opposition control), the transpiration velocities computed from Eq. (2) with A = 1 are still significantly lower than the u_y values at y + 15. This can be due to the fact that the shear stress fluctuations in the denominator of Eq. (2) are long-time averaged values taken from the uncontrolled case, while the shear stress fluctuations in the numerator of Eq. (2) are instantaneous (albeit plane-averaged) and are from the controlled case. Unfortunately, defining the shear stress fluctuations in the numerator of Eq. (2) with respect to the time-averaged value of the uncontrolled case might be misleading, as the shear stress will vary in time with control, which might result in the situation when only blowing, or only suction is used, leading to a violation of the mass

conservation in the system. This explains why increasing the gain of control (e.g., to A=4) results in higher injection velocities and to a higher control effectiveness. With A=65, the wall velocities are almost as high as the opposition control wall velocity values in Fig. 19, however, the observed instabilities in the system discussed earlier, propel us to resort to a freezing of control inputs, which likely reduces the effectiveness of the methods as compared to 'continuous' approaches that do not introduce temporal freezing. Future work will examine the strategies for effective gain increases in wall-sensing method without the need for a temporal freezing, e.g., implementing a feedback control loop based on filtered shear stress fluctuations at certain frequencies.

In our study of turbulent flow control using wall information, even though our skin friction drag reduction didn't match the effectiveness of opposition control, it's still a notable step forward in the field. First and foremost, utilization of the wall information is necessary for designing passive wall adaptation methods (such as selectively-tuned compliant surfaces or metamaterials), and the current results demonstrate a potential effectiveness of this approach, with a significant value of drag reduction of 10.64% and 7.12% achieved at friction Reynolds numbers of $Re_{\tau} = 180$ and 390, respectively, obtained 'at a first try', without any optimization of the approach. Additionally, our study reveals the potential for even greater drag reduction by effectively dampening the high-frequency fluctuations inherent in our control process.

V. Conclusion

In this study, we explored a wall-sensing method based on wall shear stress for turbulent flow control and compared it with the opposition control method, which uses velocity sensing at an off-wall location. Our results highlight the comparative effectiveness of these two methods for drag reduction at different Reynolds numbers.

In the opposition control method, we observed significant drag reduction, achieving 21.11% at $Re_{\tau} \approx 180$ and 18% at $Re_{\tau} \approx 390$. These results were obtained by capturing instantaneous velocity signals at $y^+ = 15$ (as the most effective sensing plane location in our study) and resupplying them with the opposite sign at the wall. The results from the opposition control method align with the previous literature [1, 11, 17–19].

Conversely, the wall-sensing method, which utilizes wall shear stress data, showed less effective drag reduction, with 10.64% at $Re_{\tau} \approx 180$ and 7.12% at $Re_{\tau} \approx 390$. The primary challenge with this method was the presence of high-frequency outliers in the wall shear stress data, which led to the instabilities in the feedback control loop. To mitigate this, we employed a 'freeze' technique, fixing the control inputs for a certain period of time and repeating the cycle, to allow the flow to stabilize. While this ad-hoc method improved stability and enabled higher drag reduction, it also highlighted the need for more robust control strategies to handle high-frequency fluctuations effectively.

While the wall-sensing method offers a viable approach for drag reduction, its current limitations necessitate further refinement, especially in handling high-frequency outliers. This could be mitigated by using the frequency-tuned approaches, where specific frequency bands are targeted and interfered with, instead of acting on all frequencies in the signal spectrum. These approaches will be investigated in our future work.

Acknowledgments

This work was supported by the US Air Force Office of Scientific Research under the grant number FA9550-23-1-0762, with Dr. Gregg Abate as the program manager. Partial support by NSF CBET-1944568 grant is also acknowledged.

Appendix

The turbulent statistics that involve pressure variables (rarely reported) against the MKM data in [16] for $Re_{\tau} \approx 180$ are presented in Fig. 22 to Fig. 25.

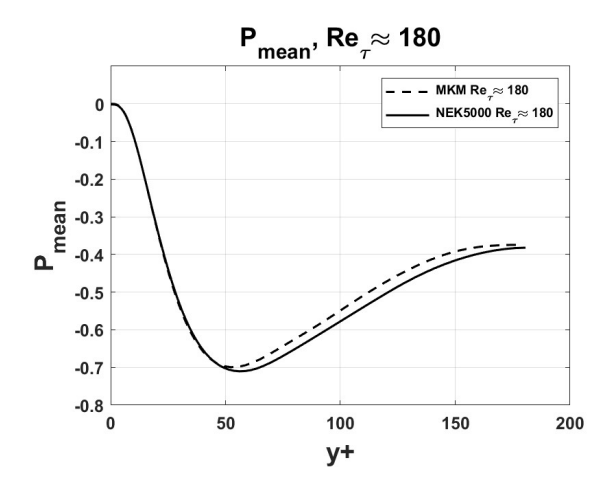
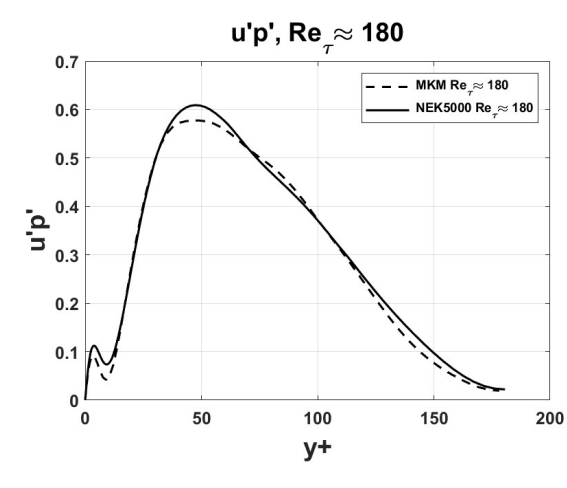


Fig. 22 P_{mean} against MKM data [16]

Fig. 23 p'p' against MKM data [16]



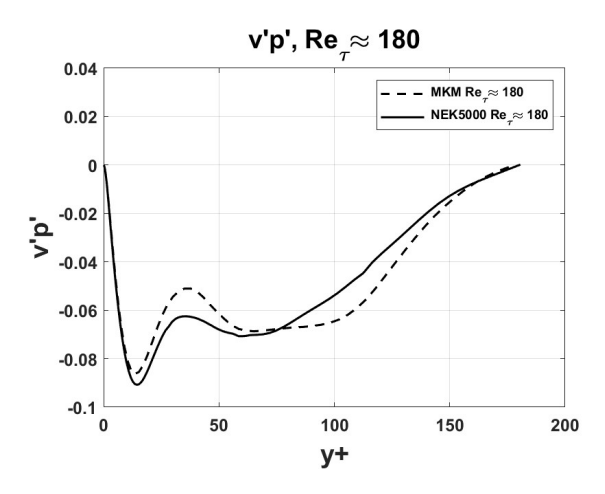


Fig. 24 u'p' against MKM data [16]

Fig. 25 v'p' against MKM data [16]

The turbulent statistics that involve pressure variables (rarely reported) against the MKM data in [16] for $Re_{\tau} \approx 390$ are presented in Fig.26 to Fig. 29.

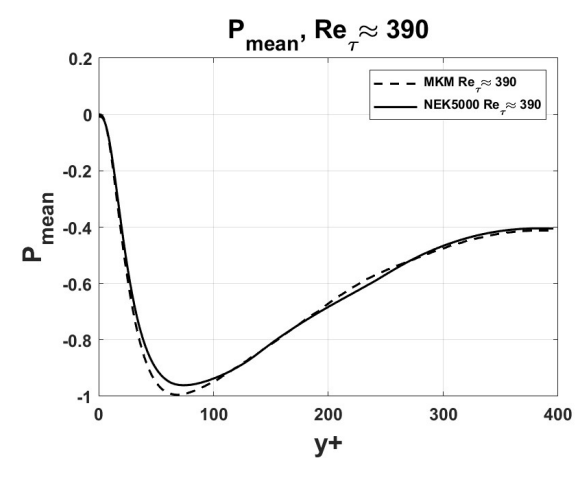


Fig. 26 P_{mean} against MKM data [16]

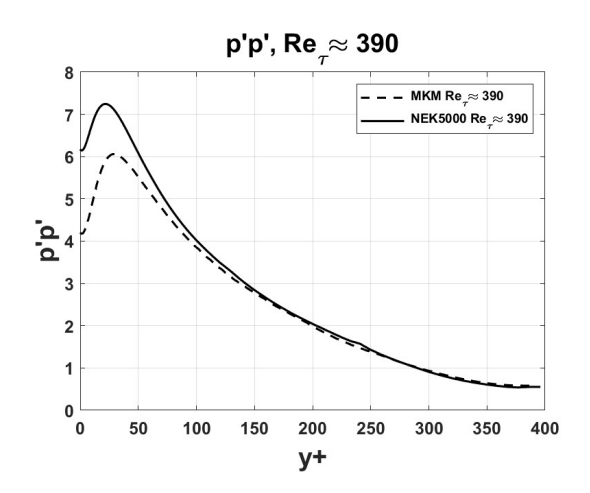
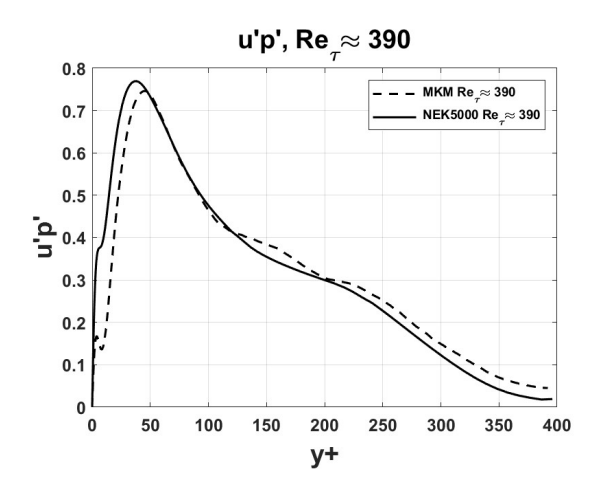


Fig. 27 p'p' against MKM data [16]



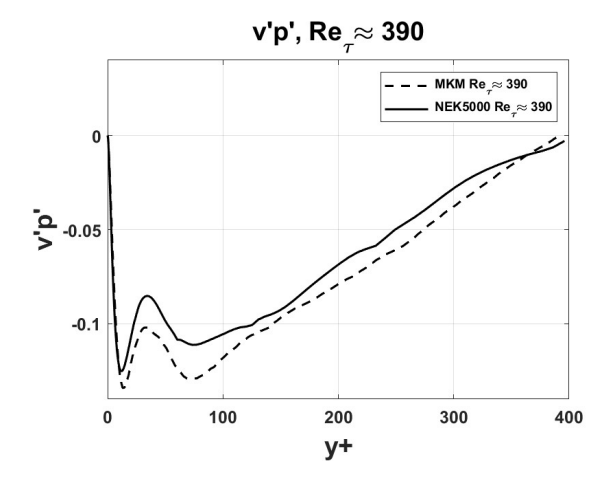


Fig. 28 u'p' against MKM data [16]

Fig. 29 v'p' against MKM data [16]

References

- [1] Choi, H., Moin, P., and Kim, J., "Active turbulence control for drag reduction in wall-bounded flows," *Journal of Fluid Mechanics*, Vol. 262, 1994, p. 75–110. https://doi.org/10.1017/S0022112094000431.
- [2] Schatz, M., Thiele, F., Petz, R., and Nitsche, W., "Separation control by periodic excitation and its application," 2nd AIAA Flow Control Conference, 2004, p. 2507. https://doi.org/10.2514/6.2004-2507.
- [3] Huang, L., Huang, P., LeBeau, R., and Hauser, T., "Numerical study of blowing and suction control mechanism on NACA0012 airfoil," *Journal of Aircraft*, Vol. 41, No. 5, 2004, pp. 1005–1013.
- [4] Zhang, S., and Zhong, S., "Turbulent flow separation control over a two-dimensional ramp using synthetic jets," *AIAA journal*, Vol. 49, No. 12, 2011, pp. 2637–2649.
- [5] You, D., and Moin, P., "Active control of flow separation over an airfoil using synthetic jets," *Journal of Fluids and Structures*, Vol. 24, No. 8, 2008, pp. 1349–1357.
- [6] Cerretelli, C., and Kirtley, K., "Boundary layer separation control with fluidic oscillators," *Journal of Turbomachinery*, Vol. 131, No. 4, 2009, p. 041001.
- [7] Gad-el-Hak, M., "Compliant coatings for drag reduction," *Progress in Aerospace Sciences*, Vol. 38, No. 1, 2002, pp. 77–99. https://doi.org/https://doi.org/10.1016/S0376-0421(01)00020-3, URL https://www.sciencedirect.com/science/article/pii/S0376042101000203.
- [8] Hussein, M. I., Biringen, S., Bilal, O. R., and Kucala, A., "Flow stabilization by subsurface phonons," *Proceedings of the Royal Society A: Mathematical, Physical and Engineering Sciences*, 2015. https://doi.org/10.1098/rspa.2014.0928.
- [9] Kang, S., and Choi, H., "Active wall motions for skin-friction drag reduction," *Physics of Fluids PHYS FLUIDS*, Vol. 12, 2000, pp. 3301–3304. https://doi.org/10.1063/1.1320833.
- [10] Pamies, M., Garnier, E., Merlen, A., and Sagaut, P., "Response of a spatially developing turbulent boundary layer to active control strategies in the framework of opposition control," *Physics of Fluids*, Vol. 19, 2007, p. 198102. https://doi.org/10.1063/1.2771659.
- [11] Lee, C., Kim, J., and Choi, H., "Suboptimal control of turbulent channel flow for drag reduction," *Journal of Fluid Mechanics*, Vol. 358, 1998, p. 245–258. https://doi.org/10.1017/S002211209700815X.
- [12] Kasagi, N., Suzuki, Y., and Fukagata, K., "Microelectromechanical systems-based feedback control of turbulence for skin friction reduction," *Annual Review of Fluid Mechanics*, Vol. 41, 2008, pp. 231–251. https://doi.org/10.1146/annurev.fluid. 010908.165221.
- [13] Fischer, P., Lottes, J., Kerkemeier, S., Marin, O., Heisey, K., Obabko, A., Merzari, E., and Peet, Y., "Nek5000: User's manual," *ANL Report No. ANL/MCS-TM-351*, 2015. Availabel on https://nek5000.mcs.anl.gov/.

- [14] Deville, M. O., Fischer, P. F., and Mund, E. H., "High-Order Methods for Incompressible Fluid Flow," *Applied Mechanics Reviews*, Vol. 56, No. 3, 2003, pp. B43–B43. https://doi.org/10.1115/1.1566402, URL https://doi.org/10.1115/1.1566402.
- [15] Fischer, P. F., "An overlapping Schwarz method for spectral element solution of the incompressible Navier Stokes equations," *Journal of Computational Physics*, Vol. 133, No. 1, 1997, pp. 84–101. https://doi.org/10.1006/jcph.1997.5651.
- [16] Moser, R., Kim, J., and Mansour, N., "Direct numerical simulation of turbulent channel flow up to Re_{τ} =590," *Physics of Fluids*, Vol. 11, 1999, pp. 943–945. https://doi.org/10.1063/1.869966.
- [17] Hammond, E. P., Bewley, T. R., and Moin, P., "Observed mechanisms for turbulence attenuation and enhancement in opposition-controlled wall-bounded flows," *Physics of Fluids*, Vol. 10, No. 9, 1998, pp. 2421–2423.
- [18] Chang, Y., Collis, S. S., and Ramakrishnan, S., "Viscous effects in control of near-wall turbulence," *Physics of Fluids*, Vol. 14, No. 11, 2002, pp. 4069–4080.
- [19] Chung, Y. M., and Talha, T., "Effectiveness of active flow control for turbulent skin friction drag reduction," *Physics of Fluids*, Vol. 23, No. 2, 2011.